International Journal of Non-Linear Mechanics 133 (2021) 103719

Contents lists available at ScienceDirect

International Journal of Non-Linear Mechanics

journal homepage: www.elsevier.com/locate/nlm

Frequency–amplitude response of superharmonic resonance of second order of electrostatically actuated MEMS cantilever resonators

Dumitru I. Caruntu *, Martin A. Botello, Christian A. Reyes, Julio Beatriz

University of Texas Rio Grande Valley, Mechanical Engineering Department, Edinburg, TX 78539, USA

ARTICLE INFO

Keywords:
Superharmonic resonance of second order
MEMS cantilever resonator
Electrostatic actuation
Method of multiple scales (MMS)
Reduced order model (ROM)
Boundary value problem (BVP)
Fringe effect
Frequency–amplitude response

ABSTRACT

This paper deals with the frequency–amplitude response of superharmonic resonance of second order (order two) of electrostatically actuated Micro-Electro-Mechanical System (MEMS) cantilever resonators. The structure of MEMS resonators consists of a cantilever resonator over a parallel ground plate, with a given gap in between, and under *AC* voltage. This resonance results from hard excitations and *AC* voltage frequency near one-fourth of the natural frequency of the resonator. The forces acting on the resonator are the nonlinear electrostatic force to include fringe effect, and a linear damping force. In order to solve the dimensionless partial differential equation of motion along with boundary and initial conditions, two types of models are developed, namely Reduced Order Models (ROMs), and Boundary Value Problem (BVP) model. The BVP model is essentially a finite difference model with a discretization in time only. ROMs are developed using one through five modes of vibration. The Method of Multiple Scales (MMS), numerical integrations using MATLAB, as well as a continuation and bifurcation analysis are used to solve the ROMs. The BVP model, resulting from using finite differences for time derivatives, is also numerically integrated. Five modes of vibration ROM is found to make accurate predictions in all amplitudes. A softening effect of the response is predicted. The response consists of a bifurcation with a bifurcation point of amplitude one fourth of the gap, and a stable branch in larger frequencies with a pull-in instability end point at three fourths of the gap. The bifurcation point shifts to lower frequencies as the voltage and/or fringe effect increase, and/or damping decreases. If damping increases, the branches coalesce, peak amplitude decreases, and a linear behavior is experienced.

1. Introduction

Applications of Micro-Electro-Mechanical Systems (MEMS) are micromotors, microswitches, microrelays, microresonators, micromirrors, micropumps, microvalves, and microfilters [1–4]. MEMS offer benefits such as low power draw requirements and physical space-saving [2]. These benefits translate to applications in the medical field such as body sensor network and micropumps for drug delivery. MEMS can be used as body sensor network connected wirelessly to a central processing hub [3]. This system has biomedical applications such as motion monitoring and bio-signal collection of vital parameters. Such applications are useful for sport, fitness, and healthcare. MEMS can also be used as integrated drug delivery systems, which incorporate a drug reservoir, micropumps, valves, microsensors, and microchannels [4]. The key components in these applications are microsensors. They provide feedback to the system. The structure of MEMS resonator consists of beam-type or plate-type flexible structure suspended over a parallel ground plate, and under Alternating Current (AC) voltage, Direct Current (*DC*) voltage, or both [1].

In order to understand the behavior, operating range, and limitations of MEMS resonators, mathematical models are needed [5]. Euler–Bernoulli beam theory is sufficient to investigate slender uniform cantilever structures [6]. At the micro-level, forces such as fringe effect and damping are no longer negligible. The fringe effect is an additional electrostatic force due to electric field outside the volume between the parallel plates [7]. The fringe effect becomes more significant with increasing the gap distance between the beam and ground plate, decreasing the width of the beam, or both. The electrostatic force and the fringe effect produce a nonlinear behavior to include bifurcations and pull-in instabilities [8]. Pull-in occurs when the electrostatic force exceeds the mechanical restoring force, and consists of contact between the tip of the cantilever resonator and the parallel ground plate [9–11]. Thus, mathematical models need to be developed in order to identify and understand the behavior of the system, in general, and pull-in phenomenon in particular. It has been shown that different mathematical models can accurately investigate pull-in instability within the dynamics of MEMS cantilevers [12–14]. Microcantilever beams were modeled using the couple stress theory along with Galerkin method in order to predict the DC pull-in voltage [12]. Node and domain transformation methods of reduced order model [13] were used to investigate clamped–clamped (bridge) microbeam resonators. When compared to

* Corresponding author.
E-mail addresses: dumitru.caruntu@utrgv.edu, caruntud2@asme.org (D.I. Caruntu).

https://doi.org/10.1016/j.ijnonlinmec.2021.103719
Received 28 February 2020; Received in revised form 19 January 2021; Accepted 18 March 2021
Available online 24 March 2021
0020-7462/

experimental data, the domain transformation method predicted the pull-in voltage. Shooting and perturbation methods were used to analyze the frequency-amplitude response of MEMS bridge microbeam resonators [14]. Reduced order models up to five modes of vibration were used and solved using a continuation and bifurcation method (AUTO 07P software package) to predict the frequency-amplitude response of parametric resonance of electrostatically actuated MEMS cantilever resonators [15].

The electrostatic force is the attraction force between the MEMS resonator and parallel ground plate and it is due to the applied voltage. The voltage can be manipulated through its magnitude and its frequency if *AC* voltage, which are two factors that can influence the behavior of the system [16].

Superharmonic resonance of second order (order two) of electrostatically actuated MEMS structures have been reported in the literature. Ghayes et al. [17] investigated the nonlinear size-dependent behavior of electrically actuated (AC voltage superimposed on a DC voltage) MEMS bridge microbeam resonators based on the modified couple stress theory. A high-dimensional reduced order model was obtained using the Galerkin method. The pseudo-arclength continuation technique was employed to investigate the behavior of the system under primary and superharmonic excitations. The frequency- and voltage-amplitude response curves of the system were constructed. The effect of taking into account the length-scale parameter on the dynamic behavior of the system was investigated by comparing the predictions of classical and modified couple stress theories. Abdel-Rahman and Nayfeh [18] reported the response of a bridge microbeam resonator sensor under superharmonic and subharmonic electric actuations. The model incorporated nonlinearities due to moderately large displacements and electric forces. The method of multiple scales was used. Both, frequency–response and voltage–response curves predicted the coexistence of multivalued solutions. The solution corresponding to a superharmonic excitation consisted of three branches meeting at two saddle–node bifurcation points and showing a hardening effect for bridges. Caruntu et al. [19] investigated the voltage–amplitude response of superharmonic resonance of second order (order two) of MEMS cantilever resonators under hard AC electrostatic actuation. AC frequency was near one-fourth of the natural frequency of the cantilever. The electrostatic force included fringe effect. Reduced Order Models (ROMs), and Boundary Value Problem (BVP) model, were used. The voltage–amplitude response showed a softening effect and three saddle–node bifurcation points. They reported that the pull-in voltage was not affected by damping or detuning frequency. Najar et al. [20] used a discretization technique combining the differential quadrature method (DQM) and the finite difference method (FDM) for the space and time in order to investigate the dynamic behavior of an electrostatic bridge microbeam actuator. They accounted for system nonlinearities due to mid-plane stretching and electrostatic force. Limit-cycle solutions of the microactuator were investigated using the nonlinear algebraic system resulted from DQM–FDM. Floquet theory and/or longtime integration were used to assess the stability of these solutions. The method was applied for large excitation amplitudes and large quality factors for secondary resonances of the first mode. They showed that DQM–FDM technique improves convergence of the dynamic solutions. Nayfeh and Younis [21] investigated the dynamics of electrically actuated bridge microbeam resonators under secondary resonance excitations. The microbeams were excited by DC voltage, and AC voltage with a frequency tuned near half their fundamental natural frequencies (superharmonic excitation of order two). The effects of varying the DC bias, damping, and AC excitation amplitude on the frequency–response curves have been reported. The *DC* bias was significantly larger than the *AC* voltage. They also reported that the dynamic pull-in instability can occur at an electric load much lower than a purely DC voltage and of the same order of magnitude as that in the case of primary-resonance excitation. Al-Ghamdi et al. [22] experimentally investigated the primary, superharmonic of order two, and subharmonic of order one-half resonances of electrostatic MEMS actuators consisting of two parallel cantilevers with an end plate under direct electrostatic excitation. The experiments were conducted in soft vacuum to reduce squeeze-film damping, and the actuator response was measured optically using a laser vibrometer. Alsaleem et al. [23] reported on modeling and experimental investigation of nonlinear resonances of electrostatically actuated resonators consisting of two cantilever beams with a proof mass attached to their tips. A nonlinear forcing composed of a DC parallel-plate electrostatic load superimposed on an AC harmonic load was used. Investigations of primary, superharmonic and subharmonic resonances, as well as dynamic pull-in, were conducted. A nonlinear spring–mass–damper model accounting for squeeze-film damping and the parallel-plate electrostatic force was utilized. Safety and integrity of MEMS resonators based on the simulated basin of attraction and the observed experimental data were reported. Ibrahim et al. [24] reported on the dynamics of cantilever microbeams under multiple harmonic electrostatic excitation frequencies. The response of microcantilevers were simulated for primary resonance, and secondary resonances, namely superharmonic of order two and subharmonic of order one half. Galerkin method has been used to develop a reduced order model. The response under three AC sources excitation was investigated.

In conclusion, superharmonic resonances were reported in the literature for electrostatically actuated MEMS microbeam resonators, namely microbridges (clamped–clamped) [17,18,20,21], microcantilevers (clamped-free) [19,24], and lumped models [22,23]. The superharmonic resonance occurred at two different AC frequencies, depending on the voltage, i.e. the case of AC only, and the case of both DC and AC. An important distinction is that, if the actuating voltage consisted of AC component only [19], then the superharmonic resonance of second order occurred for AC frequency near one fourth of the natural frequency of the resonator. If the actuating voltage included both components DC and AC, in which the DC voltage was much larger than the AC voltage [17,18,20–24], then the superharmonic resonance of second order occurred for AC frequency near one half of the natural frequency. Reference [19] reported only the voltage–amplitude response. Frequency–amplitude responses of electrostatically actuated microbridges [17,18,20,21], and microcantilevers [24] have been reported in the literature.

Present work is an extension of Caruntu et al. [19] and reports the nonlinear frequency–amplitude response of superharmonic resonance of second order of electrostatically actuated MEMS cantilever resonators. The applied *AC* voltage is in the realm of hard excitation with the frequency near one-fourth natural frequency. A resonance for *AC* frequency as low as one-fourth of natural frequency is a very important benefit of this work, when compared to other studies that include a DC voltage larger than the AC voltage of frequency near half natural frequency to produce the same type of resonance. Two different models of investigation result from transforming the dimensionless partial differential equation into an ordinary differential equation, or a system of ordinary differential equations. The first type of models are ROMs, which are based on Galerkin procedure [11,15,25]. ROMs use the modes of vibration of the resonator. Specifically, they use the mode shapes as a basis of functions. ROMs consist of a system of ordinary differential equations in time along with initial conditions. The size of the system depends on the number of modes of vibration used. The second model is a BVP model in which the time derivatives of the dimensionless partial differential equation of motion are replaced by finite differences. This way, the model results in a system of BVPs, i.e. one BVP at each step in time. These models are solved using either analytical or numerical methods.

To the authors' best knowledge, this is the first time when (1) the frequency–amplitude response of superharmonic resonance of second order of electrostatically actuated MEMS cantilever resonators subjected to hard excitations, with (2) an AC frequency near one fourth of the natural frequency, and (3) using several methods of

investigation, is reported. (4) Present research predicts the existence of pull-in for this resonance for a range of frequencies. Only two other investigations reported on superharmonic resonance of electrostatically actuated MEMS cantilever resonators. One investigation reported only on voltage–amplitude response [19]. The other investigation used both DC voltage and small AC voltage with a frequency near half natural frequency [24], not one fourth as in this paper, and did not predict the unstable branches in the response; moreover, they reported only a very particular dimensional case. Present research uses the Method of Multiple Scales (MMS) for solving one mode of vibration ROM and predicting the frequency–amplitude response. Two through five modes of vibration ROMs are solved using AUTO 07P, a continuation and bifurcation software, to predict the frequency–amplitude bifurcation diagram. A convergence investigation shows that ROM with five modes of vibration should be used for both small and large (compared to the gap) amplitudes. This is similar to Caruntu et al. [19]. The five term ROM is also numerically integrated in MATLAB to predict time responses of the structure. Moreover, BVP model is numerically integrated in MATLAB and used to predict time responses of the structure as well. The only other work investigating superharmonic resonance of electrostatically actuated MEMS cantilever resonators reported in the literature and using ROMs and BVPs models, and methods such as MMS, direct numerical integration, and AUTO 07 for continuation and bifurcation is Ref. [19] which reported only the voltage–amplitude response. (5) Present work reports that MMS is valid for amplitudes less than 0.1 of the gap, and unreliable for larger amplitudes. ROM and BVP models are valid for all range of amplitudes provided that a sufficient number of modes of vibration used in the ROM, and small enough *timestep* size for BVP are considered. Five modes of vibration ROM accurately predicts the frequency–amplitude response of the system. In Ref. [24], the authors reported only time responses resulting from numerical integration of ROM with at least three modes of vibration. This approach did not provide the unstable branches in the response. Also, they did not report a convergence study by the number of modes of vibration in order to determine the necessary number of modes in the ROM. "While Abdel-Rahman and Nayfeh [18] used the method of multiple scales, Nayfeh and Younis [21], and Ghayesh et al. [17], used reduced order models to include 4 and 16 modes of vibration, respectively. However, neither Ghayesh et al. [17] nor Nayfeh and Younis [21] reported a convergence criterion for determining the number of modes of vibration necessary in the model" [19]. (6) The effect of voltage, fringe, and damping on the amplitude–frequency response are also reported. These effects on superharmonic resonance of second order of electrostatically actuated MEMS cantilever resonators were reported in Ref. [19], yet only on the voltage-amplitude response. These effects were not reported in Ref. [24]. Their model did not include the fringe effect, the AC voltage was much less than the DC voltage, and the work rather focused on multi-frequency excitations.

2. Partial differential equation of motion

The motion of electrostatically actuated Euler–Bernoulli cantilever resonator, Fig. 1, is given by the following dimensionless partial differential equation, and boundary and initial conditions [11,19,26]

$$\begin{cases} \frac{\partial^2 u}{\partial \tau^2} + b^* \frac{\partial u}{\partial \tau} + \frac{\partial^4 u}{\partial z^4} = \frac{\delta \cdot V^2}{(1-u)^2} + \frac{f\delta \cdot V^2}{(1-u)} \\ u(0,\tau) = \frac{\partial u}{\partial z}(0,\tau) = \frac{\partial^2 u}{\partial z^2}(1,\tau) = \frac{\partial^3 u}{\partial z^3}(1,\tau) = 0 \\ u(z,0) = f(z), \frac{\partial u}{\partial \tau}(z,0) = g(z) \end{cases} \tag{1}$$

where $u = u(z,\tau)$, z, and τ are dimensionless transverse displacement (deflection) of the resonator, dimensionless longitudinal coordinate, and dimensionless time, respectively. They are given by

$$u = \frac{w}{g}; \quad z = \frac{x}{\ell}; \quad \tau = t \cdot \frac{1}{\ell^2}\sqrt{\frac{EI_0}{\rho A_0}} \tag{2}$$

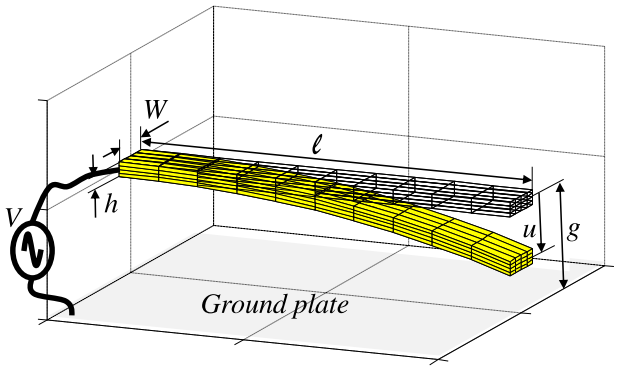

Fig. 1. Uniform cantilever beam MEMS resonator under electrostatic actuation.

where w is the dimensional transverse displacement of the cantilever, x dimensional longitudinal coordinate, t dimensional time, ℓ beam length, g gap between the cantilever and ground plate, ρ density, and E Young modulus. A_0 and I_0 are the cross-section area and moment of inertia of the cantilever, respectively. Functions $f(z)$ and $g(z)$ are the initial deflection and velocity of the resonator, respectively. In the present work only *AC* voltage is considered. The dimensionless *AC* voltage $V(\tau)$ is as follows

$$V(\tau) = \cos \Omega^* \tau \tag{3}$$

The dimensionless parameters in Eq. (1) are b^* dimensionless damping parameter, δ dimensionless amplitude of the electrostatic excitation force (or dimensionless voltage) parameter, and f dimensionless fringe parameter, Ω^* dimensionless frequency of excitation, and ω_i dimensionless ith natural frequency. They are given by

$$b^* = \frac{b\ell^2}{g\sqrt{\rho E A_0 I_0}}, \quad \delta_i = \frac{\varepsilon_0 W \ell^4 V^2}{2g^3 E I_0}, \quad f = \frac{0.65g}{W},$$
$$\Omega^* = \Omega \ell^2 \sqrt{\frac{\rho A_0}{E I_0}}, \quad \omega_i = \overline{\omega}_i \ell^2 \sqrt{\frac{\rho A_0}{E I_0}} \tag{4}$$

where b is viscous damping per unit length, W beam width, ε_0 permittivity of free space, Ω dimensional frequency of excitation, and $\overline{\omega}_i$ dimensional ith natural frequency.

Palmer's formula [7,19,26,27] consisting of the two terms at the right-hand side of Eq. (1) is used for the electrostatic force including the fringe effect. This formula holds for structures that do not fall in the category of narrow beams.

Regarding damping, a variety of sources such as air damping, acoustic radiation, support loss, phonon scattering, and thermoelastic loss can contribute to the overall damping of a MEMS resonator [28]. However, depending on the operating condition of the system, different loss mechanisms are more dominant. In this paper, it is assumed that the dominant damping loss is due to air damping. For MEMS, there are four regimes of air damping: (1) intrinsic, (2) rarefied, (3) viscous, and (4) squeeze film [28]. Intrinsic and rarefied regimes are at relative high vacuum of less than 10 Pa and between 10–1000 Pa, respectively. Viscous and squeeze film fall under pressure values between 1000 Pa – 1 atm. The quality factor Q and the damping coefficient per length b [29–32] in present work are for damping in rarefied gas, [29].

3. Superharmonic resonance of second order

The dimensionless frequency Ω^* of the *AC* voltage between the cantilever and the parallel ground plate is near one fourth of the first dimensionless natural frequency $\Omega^* \approx \omega_1/4$, [19]. Using σ as a frequency detuning parameter, and ε as a dimensionless parameter

utilized as a bookkeeping device in MMS to indicate small terms of the equation, the *AC* voltage frequency can be written as

$$\Omega^* = \frac{\omega_1}{4} + \varepsilon\sigma \tag{5}$$

Considering small damping, Eq. (1) can be written as

$$\frac{\partial^2 u}{\partial \tau^2} + \varepsilon b^* \frac{\partial u}{\partial \tau} + \frac{\partial^4 u}{\partial z^4} = \left[\frac{\delta}{(1-u)^2} + \frac{f\delta}{(1-u)}\right] V^2 \tag{6}$$

One should mention that the voltage parameter δ should be large enough to produce hard excitations in order for this resonance to occur.

4. Method of multiple scales

MMS is used in this work to investigate the frequency–amplitude response of superharmonic resonance of second order of electrostatically actuated cantilever resonators. In Eq. (6), the nonlinear electrostatic force and fringe effect are expanded in Taylor series and terms up to the cubic power are retained. The solution of the resulting equation is assumed as $u = u_1(\tau)\phi_1(z)$, where $\phi_1(z)$ is the mode shape of the first mode of vibration and u_1 is a function of time to be determined. The mode shapes $\phi_i(z)$ of a beam satisfy the orthonormality conditions [19]. Using the Taylor expansions up to cubic powers, and in order to model hard excitations, Eq. (6) becomes

$$\ddot{u}_1\phi_1 + \varepsilon b^*\dot{u}_1\phi_1 + \omega_1^2 u_1\phi_1 = c_1\delta V^2 + \varepsilon\delta V^2 \sum_{k=1}^{3} c_{k+1} u_1^k \phi_1^k \tag{7}$$

where ω_1 is the first natural frequency, and $c_n = n + f$, $n = 1, 2, 3, 4$. The bookkeeping parameter ε [33,34] indicates small terms in Eq. (7). The first term on the right hand side of Eq. (7), namely $c_1\delta V^2$, term belonging to the electrostatic force, does not contain the bookkeeping parameter ε while all other terms of the Taylor polynomial contain ε. This is the way hard electrostatic excitations are MMS modeled in this work. As opposed to this case, in the case of soft excitation, i.e. the electrostatic force is relatively small, all terms at the right-hand side of Eq. (7) contain ε including $c_1\delta V^2$. Assume a uniform expansion [35] of u_1 as $u_1 = u_{10}(T_0, T_1) + \varepsilon u_{11}(T_0, T_1)$, where the fast-time scale and the slow-time scale [15], are $T_0 = t$ and $T_1 = \varepsilon t$, respectively. After multiplying Eq. (7) by ϕ_1 and integrating from zero to one, the uniform expansion is substituted into the resulting equation. Then, equating the coefficients of the same powers of ε, the following two problems, namely zero-order and first-order, result [19]

$$\text{Order } \varepsilon^0: \; D_0^2 u_{10} + \omega_1^2 u_{10} = c_1 g_0 \delta V^2 \tag{8}$$

$$\text{Order } \varepsilon^1: \; D_1^2 u_{11} + \omega_1^2 u_{11} = -2D_0 D_1 u_{10} - b^* D_0 u_{10} + \delta V^2 \sum_{k=1}^{3} c_{k+1} g_k u_1^k \tag{9}$$

where $D_n = \frac{\partial}{\partial T_n}$, $n = 1, 2$, and $g_n = \int_0^1 \phi_1^{n+1} dz$, $n = 1, 2, 3$. Due to the orthonormality property of the mode shapes, $g_1 = 1$. Solving Eq (8) and substituting the solution in Eq. (9), collecting the secular terms (terms containing $e^{i\omega_1 T_0}$) from the resulting equation and setting their sum equal to zero, the steady-state solutions (steady amplitude $a' = 0$ and steady phase $\gamma' = 0$) result as follows [19]

$$\begin{aligned}\sigma = &-\frac{\delta}{4\omega_1}\left[\frac{1}{4}c_2 + \frac{1}{2}(K+\Lambda)c_3 g_2 \right.\\ &\left. + \left(\frac{3}{16}a^2 + \frac{3}{4}K^2 + \frac{3}{2}\Lambda^2 + \frac{3}{2}\Lambda K\right)c_4 g_3\right] -\\ &\frac{\delta\Lambda cos\gamma}{4\omega_1 a}\left[\frac{1}{4}c_2 + \frac{1}{2}(\Lambda+K)c_3 g_2 + \left(\frac{9}{16}a^2 + \frac{3}{4}K^2 + \Lambda^2 + \frac{3}{2}\Lambda K\right)c_4 g_3\right]\end{aligned} \tag{10}$$

and

$$\begin{aligned}0 = &-\frac{1}{2}b^* a\omega_1 + \delta\Lambda sin\gamma\left[\frac{1}{4}c_2 + \frac{1}{2}(\Lambda+K)c_3 g_2\right.\\ &\left. + \left(\frac{3}{16}a^2 + \frac{3}{4}K^2 + \Lambda^2 + \frac{3}{2}\Lambda K\right)c_4 g_3\right]\end{aligned} \tag{11}$$

where

$$\gamma = 4\sigma T_1 - \beta, \quad \gamma' = 4\sigma - \beta' \tag{12}$$

$$\Lambda = \frac{\delta g_0(1+f)}{4\left(\omega_1^2 - 4\Omega^{*2}\right)}, \qquad K = \frac{\delta g_0(1+f)}{2\omega_1^2} \tag{13}$$

and a and β are amplitude and phase, respectively. Eqs. (10) and (11) are parametric equations, where the parameter is γ. For given voltage δ, fringe f and damping b^* parameters, the steady-state amplitude a and detuning frequency parameter σ are determined from these equations. Eqs. (10) and (11) give the (σ, a) frequency–amplitude response, or bifurcation diagram, of the superharmonic resonance of second order. The amplitude of the tip of the cantilever resonator is given by $U_{\max} = a\phi_1(1)$.

5. Reduced order models

The partial differential equation of motion is transformed into a set of non-explicit ordinary differential equations, i.e. ROMs [11] to include several modes of vibration. These models are based on the Galerkin procedure and use the undamped linear mode shapes of the cantilever beam as an orthogonal basis of functions. The ROM solution is assumed to be $u(z,\tau) = \sum_{i=1}^{N} u_i(\tau)\phi_i(z)$, where $N = 2, 3, 4, 5$ is the number of ROM terms (or modes of vibration), u_i are time dependent functions to be determined, and ϕ_i are the linear undamped mode shapes of uniform cantilever beams. The dimensionless equation of motion Eq. (1) is multiplied by $(1-u)^2$ in order to eliminate any displacement terms from appearing in the denominators [27,28]. Next, ROM solution is substituted into the resulting equation, which is then multiplied by $\phi_n(z)$ and integrated from $z = 0$ to *1*, where $n = 1, 2, \ldots, N$. This results in a ROM system of N second order differential equations as follows [19]

$$\sum_{i=1}^{N}\ddot{u}_i A_{ni} + \sum_{i=1}^{N}\omega_i^2 u_i A_{ni} + b^*\sum_{i=1}^{N}\dot{u}_i A_{ni} = \delta V^2\left(c_1 h_n + f\sum_{i=1}^{N} u_i h_{ni}\right) \tag{14}$$

where $n = 1, 2, \ldots, N$ and $i, j, k = 1, 2, \ldots, N$ and

$$\begin{aligned}&A_{ni} = h_{ni} - 2\sum_{j=1}^{N} u_j h_{nij} + \sum_{j,k=1}^{N} u_j u_k h_{nijk}, \; h_n = \int_0^1 \phi_n dz,\\ &h_{ni} = \int_0^1 \phi_i\phi_n dz, \; h_{nij} = \int_0^1 \phi_i\phi_j\phi_n dz, \; h_{nijk} = \int_0^1 \phi_i\phi_j\phi_k\phi_n dz,\end{aligned} \tag{15}$$

The system of second-order differential Eqs. (14) is then transformed into a system of first order differential equations. Four cases, namely $N = 2$, $N = 3$, $N = 4$, and $N = 5$ are investigated using AUTO 07P, a software package for continuation and bifurcation problems [36]. "In this work, time responses for specified parameters are generated using a MATLAB ODE solver, namely *ode15s*. One should mention that *ode15s* is a multistep, variable order solver based on numerical differentiation formulas (NDFs)", [19,37,38].

6. Boundary value problem model

Another model, namely the Boundary Value Problem model, is used to investigate the frequency–amplitude response of the superharmonic resonance. The initial conditions considered for the numerical simulations in this work are zero initial velocity and initial deflection u_0.

Considering a time sequence $(\tau)_n$ and denoting $u(z, \tau_n) = u_n$, the time partial derivatives of Eq. (1) are converted to difference quotients. It results a 4th order space dependent ordinary differential equation in terms of z for each step in time τ_n. The resulting system of first-order differential equations for each step in time τ_n is given by [19]

$$\begin{cases} y'_{k,n} = y_{k+1,n}\,, \quad k = 1, 2, 3\\ y'_{4,n} = -\frac{y_{1,n} - 2y_{1,n-1} + y_{1,n-2}}{(\Delta\tau)^2} - b^*\frac{y_{1,n} - y_{1,n-2}}{2\Delta\tau}\\ \quad + \frac{\delta}{(1-y_{1,n})}\left[f + \frac{1}{(1-y_{1,n})}\right]\cos^2\Omega\cdot\tau_n \end{cases} \tag{16}$$

Table 1
Dimensional system parameters.

Beam width	W	20 μm
Beam length	ℓ	300 μm
Beam thickness	h	2.0 μm
Initial gap distance	g	8.0 μm
Material density	ρ	2330 kg/m^3
Young's modulus	E	169 GPa
Permittivity of free space	ε_0	8.854×10^{-12} C^2/N-m^2
Quality factor	Q	4200
Peak AC Voltage	V_0	28.36 V

Table 2
Dimensionless system parameters.

Damping parameter	b^*	0.01
Voltage parameter	δ	0.5
Fringe correction parameter	f	0.26

Table 3
First five natural frequencies and constant coefficients for uniform cantilever.

	$i=1$	$i=2$	$i=3$	$i=4$	$i=5$
ω_i	3.51605	22.03449	61.69721	120.90192	199.85953
C_i	−0.73410	−1.01847	−0.99922	−1.00003	−0.99999

Table 4
g coefficients for Eq. (16).

	$n=0$	$n=1$	$n=2$	$n=3$
g_n	0.7830	1.0000	1.4778	2.3487

where $n=3,4,5,\ldots,$ $'$ denotes derivative with respect to z, and the four new variables for each step in time τ_n are as follows

$$y_{k,n}=\frac{d^{k-1}u_n}{dz^{k-1}},\quad k=1,2,3,4 \tag{17}$$

The boundary value problem given by Eqs. (16) along with boundary conditions is solved using *bvp4c*, a boundary value problem solver of MATLAB, for each step in time τ_n, $n=3,4,5,\ldots$. This solver is based on the three-stage Labatto formula which is a collocation formula. The collocation polynomial provides a solution that is a fourth-order accurate uniformly in $[0,1]$ in our case [39].

7. Numerical results

The superharmonic resonance of second order is investigated using the MMS, continuation and bifurcation analysis using AUTO 07 and numerical integration using Matlab of ROMs with up to five modes of vibration (5 terms), and numerical integration using Matlab of the BVP model. The effects of parameters δ, f, and b^* on the frequency–amplitude response are investigated. Tables 1 and 2 show the dimensional and dimensionless parameters of the MEMS cantilever used for numerical simulations, respectively, in the case of rarefied gas regime [19]. Table 3 gives the first five dimensionless natural frequencies and the constants of the corresponding cantilever mode shapes [8]. Table 4 gives the g-coefficients of Eqs. (10)–(13).

Fig. 2 shows the frequency–amplitude response (bifurcation diagram) in accordance with MMS, five-term (modes of vibration) ROM AUTO 07P (5T AUTO), five-term ROM time responses (5T TR) using MATLAB *ode15s*, and BVP time responses using MATLAB *bvp4c*. In the horizontal axis is the detuning frequency σ, and in the vertical axis is $U_{\max}$, the steady-state amplitude of the tip of the cantilever. The dashed and solid lines represent the unstable and stable steady-state amplitudes of the system, respectively.

A comparison between the predictions of the models and methods used in this work shows that all predictions are in agreement for amplitudes less than 0.1 of the gap. For amplitudes larger than 0.1 of the gap, only the ROM (5T TR) time responses, BVP time responses,

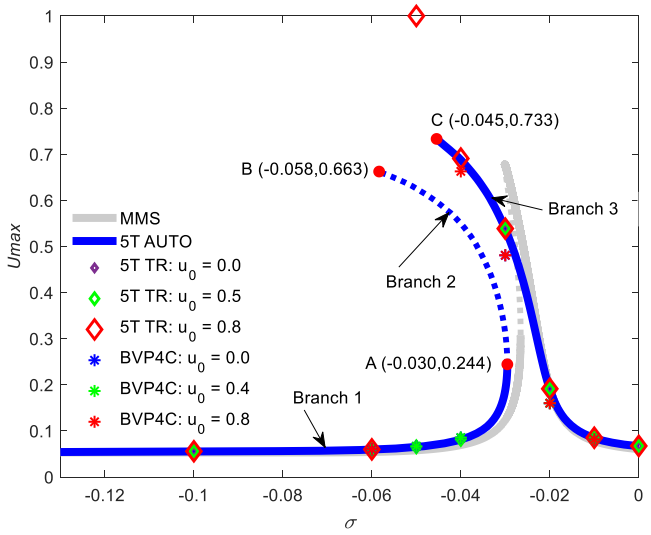

Fig. 2. Frequency–amplitude response using MMS, 5T AUTO, 5T TR, and BVP4C; $b^*=0.01$, $f=0.26$, $\delta=0.5$, $\omega_1=3.5160$, Mode 1.

and ROM (5T AUTO) AUTO 07P frequency–amplitude responses are in agreement, providing accurate predictions. MMS is inaccurate for amplitudes larger than 0.1. This is consistent with the fact that MMS is not a reliable method for strong nonlinearities and large amplitudes. Moreover, MMS uses only one mode of vibration and a third degree Taylor polynomial approximation of the electrostatic force [27,35]. However, MMS has two important benefits, it predicts the existence of these secondary resonances, and has excellent predictions for weak nonlinearities and small amplitudes. On the other hand, ROMs with a sufficient number of modes of vibration, and BVP models with sufficiently small time stepsize used for numerical integration, are reliable models for systems with strong nonlinearities and large amplitudes. ROMs and BVP model use the exact partial differential equation of motion. There is no approximation such as Taylor polynomials of the electrostatic force to include fringe effect. This way the existence of singularities of the differential equation is preserved. Also, it is known that the larger the number of modes of vibration in the ROM, the more accurate the predictions are [19]. However, the larger the number of modes of vibration in the ROM, the larger the computational time.

The frequency–amplitude response shows a softening effect (5T AUTO), i.e. branches in higher amplitudes are bent towards lower frequencies. Because the end point B of the unstable branch has a lower frequency than point C, the system experiences pull-in instability for initial deflections above the unstable branch AB when the detuning frequencies σ are between σ_B and σ_C, i.e. $-0.058\le\sigma<-0.045$. This is the first time when the pull-in phenomenon of this resonance is predicted for a range of frequencies. One can notice that MMS predicts erroneously that the system does not experience any pull-in instability in this range of frequencies.

One can see that in the case of constant frequency and constant voltage parameter $\delta=0.5$, pull-in could not be reached when the detuning frequency parameter σ is outside the interval (σ_B,σ_C), regardless the values of the initial deflection u_0. Outside this interval, the MEMS resonator settles to amplitudes on the stable branches (solid lines) 1 and 3. In the case of constant voltage parameter $\delta=0.5$ and sweeping up the frequency, the steady state amplitude stays on branch 1 at 0.05 of the gap, and then increases until it reaches bifurcation point A. At this point the stability is lost, and the steady state amplitude jumps from a value of $U_{\max}=0.244$ of the gap at point A to a value of about $U_{\max}=0.6$ of the gap on branch 3. The steady state amplitude decreases along branch 3 as the frequency continues to be swept up. When the frequency is swept down, the steady state amplitude increases along branch 3 until

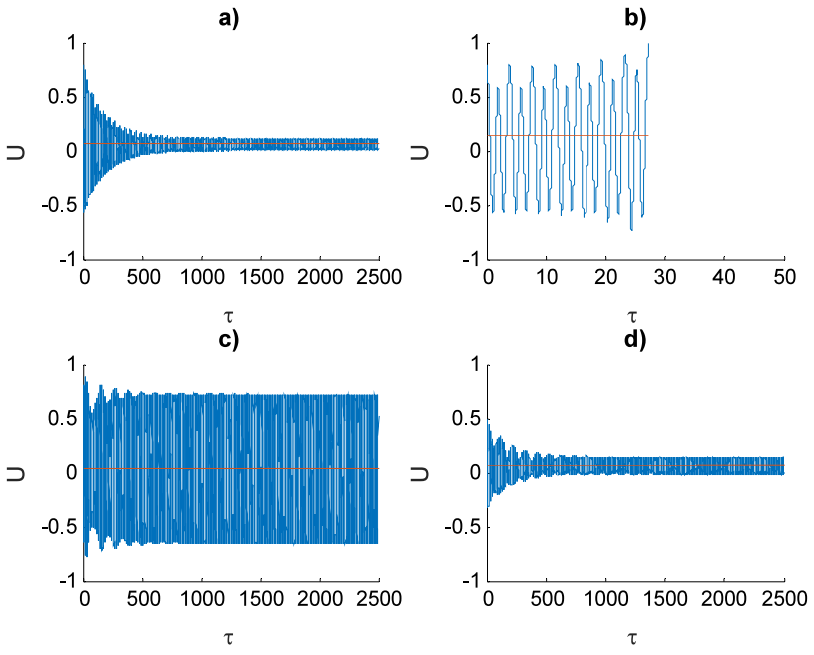

Fig. 3. Time response using five term ROM; $b^* = 0.01$, $f = 0.26$, $\delta = 0.5$; (a) $\sigma = -0.06$, $u_0 = 0.8$, (b) $\sigma = -0.05$, $u_0 = 0.8$, (c) $\sigma = -0.04$, $u_0 = 0.8$, (d) $\sigma = -0.04$, $u_0 = 0.5$.

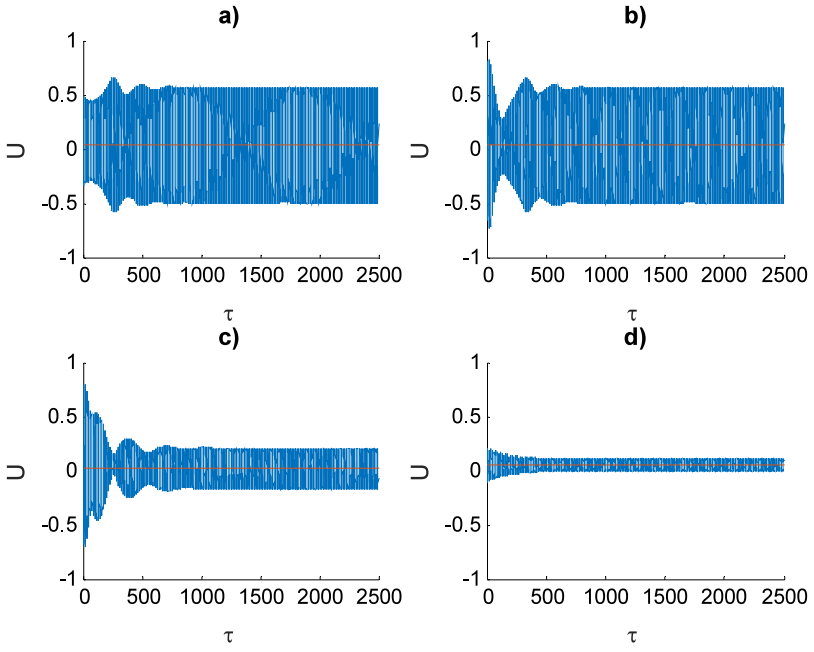

Fig. 4. Time response using five term ROM; $b^* = 0.01$, $f = 0.26$, $\delta = 0.5$; (a) $\sigma = -0.03$, $u_0 = 0.5$, (b) $\sigma = -0.03$, $u_0 = 0.8$, (c) $\sigma = -0.02$, $u_0 = 0.8$, (d) $\sigma = -0.1$, $u_0 = 0$.

it reaches point C, where the system loses stability and it experiences pull-in, the amplitude reaching the value of $U_{\max} = 1$, i.e. the MEMS cantilever resonator makes contact with the ground plate.

All time responses, Figs. 3–5, show the dimensionless deflection u of the tip of the MEMS cantilever resonator as a function of dimensionless time τ. Figs. 3 and 4 show the five-term ROM time responses. Fig. 5 shows the time response for *bvp4c* with a $timestep = 0.0005$ for $(\tau)_n$. One should mention that an investigation regarding the value of the *timestep* has been conducted. This investigation showed that for smaller values than $timestep = 0.0005$, no significant differences can be seen in the time responses.

Figs. 3a and 3b do not contradict the existence of the unstable branch 2 and the existence of the endpoint B showing that from the same initial deflection $u_0 = 0.8$, if the frequency is less thanu σ_B, the frequency of point B, the microresonator settles to a small amplitude on branch 1, and if the frequency is greater than σ_B but less than σ_C, then the microresonator experiences pull-in reaching the dimensionless deflection $u = 1$.

Figs. 3b and 3c not contradict the existence of branch 3 and the endpoint C, showing that from the same initial deflection $u_0 = 0.8$, if the frequency is less than σ_C and greater than σ_B, the microresonator experiences pull-in, and if the frequency is greater than σ_C, then the microresonator settles to an amplitude on branch 3.

Figs. 3c and 3d do not contradict the existence of the unstable branch 2, showing that for the same frequency $\sigma = -0.04$, if the initial deflection u_0 is above the unstable branch 2, then the microresonator settles to and amplitude on the stable branch 3, and if the initial

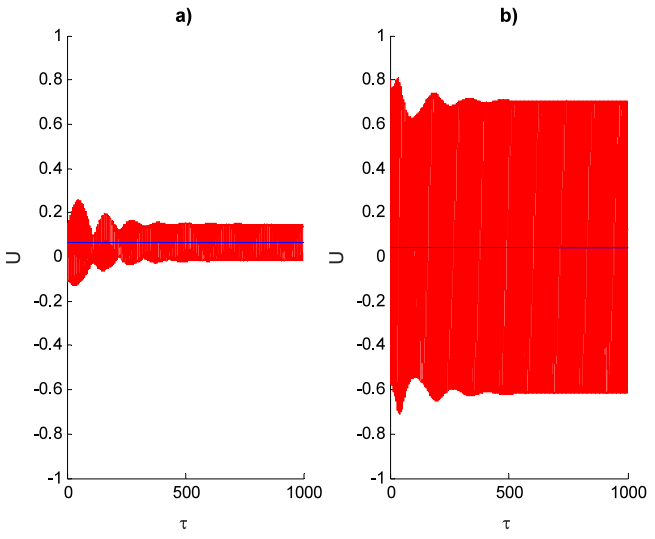

Fig. 5. Time response using five term ROM; timestep = 0.0005, $b^* = 0.01$, $f = 0.26$, $\delta = 0.5$; (a) $\sigma = -0.04$, $u_0 = 0$, (b) $\sigma = -0.04$, $u_0 = 0.8$.

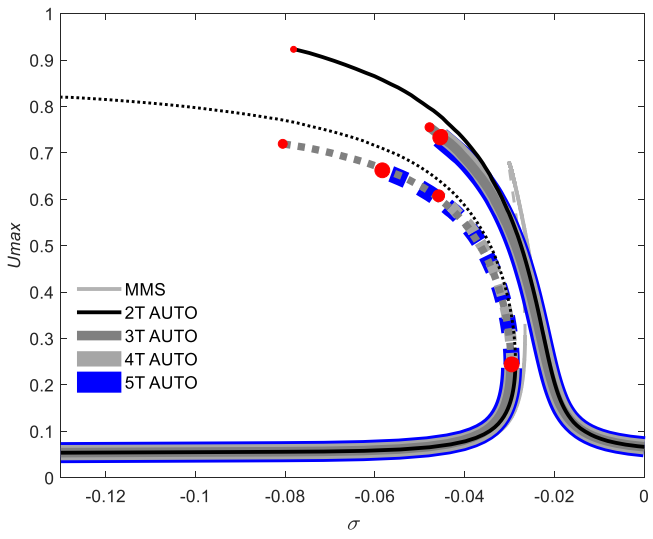

Fig. 6. Convergence of frequency–amplitude response using MMS, two, three, four, and five term ROM; $b^* = 0.01$, $f = 0.26$, $\delta = 0.5$, $\omega_1 = 3.5160$, Mode 1.

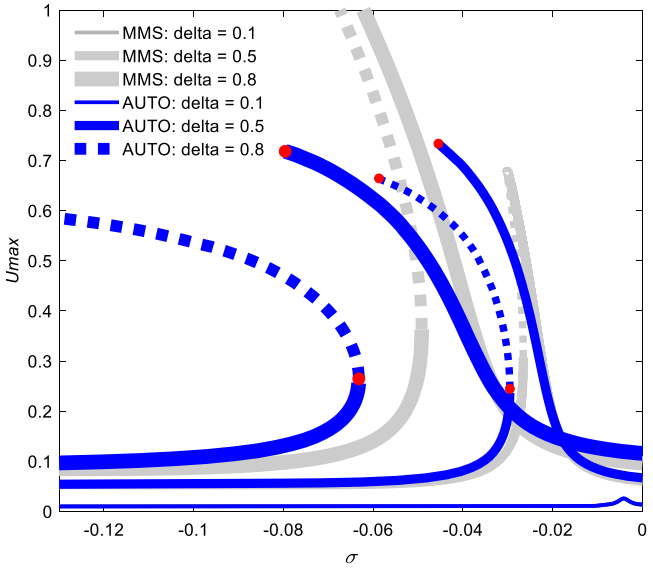

Fig. 7. Effect of damping parameter on the frequency–amplitude response using MMS and 5T AUTO; $f = 0.26$, $\delta = 0.5$, $\omega_1 = 3.5160$, Mode 1.

deflection u_0 is below the unstable branch 2, then the resonator settles to and amplitude on the stable branch 1.

Figs. 4a and 4b, and Figs. 4b and 4c, do not contradict the existence of the stable branch 3, showing (1) that for the same frequency $\sigma = -0.03$, regardless the initial deflections, $u_0 = 0.5$ or $u_0 = 0.8$, the microresonator settles to the same amplitude on branch 3, and (2) that for the same initial deflection $u_0 = 0.8$, and two different frequencies $\sigma = -0.02$ and $\sigma = -0.03$, the microresonator settles to amplitudes on the stable branch 3, respectively.

Figs. 3a and 4d do not contradict the existence of the stable branch 1 showing that for two different frequencies, both less than σ_B, and for two different initial deflections $u_0 = 0.8$ and $u_0 = 0$, the microresonator settles to amplitudes on branch 1.

Fig. 5a, with an initial deflection of $u_0 = 0$, and a detuning frequency parameter of $\sigma = -0.04$, shows a time response in agreement with Fig. 2. Fig. 5b, with an initial deflection of $u_0 = 0.8$, and a detuning frequency parameter of $\sigma = -0.04$, also shows a time response in agreement with Fig. 2.

A bias, due to hard excitations, is experienced in these time responses. The bias is given by the movement of the tip reaching greater values in the positive direction than in the negative direction. One can notice from all time responses that the amplitude due to the bias is not significant when compared to the gap.

Fig. 6 illustrates the convergence of frequency–amplitude response using two, three, four, and five terms ROM AUTO. This is necessary in order to select the number of terms in the ROM to be used in the investigation. Results using MMS are included since MMS solves one term (mode of vibration) ROM. The softening effect, i.e. bending of both branches towards lower frequencies at high amplitudes, increases with the number of terms. The end point of the unstable branch converges to point *B*, Fig. 2, and the end point of the stable branch to point *C*, Fig. 2. The softening effect, the bifurcation point *A* and the end point *C* show no significant difference between three, four, and five terms ROM AUTO, while point *B* does. Since no significant changes can be seen between four-term and five-term ROM AUTO responses, five-term ROM AUTO is used in this research to investigate system's behavior for all amplitudes.

Fig. 7 illustrates the effect of the voltage parameter δ on the frequency–amplitude response. For the voltage parameter $\delta = 0.1$, i.e. soft excitation, the system experiences a very low peak amplitude $U_{\max} = 0.015$ and linear behavior. As the system goes into hard excitations, $\delta = 0.5$ and $\delta = 0.8$, a two branch softening effect nonlinear behavior occurs. For the nonlinear behavior, as the values of the voltage parameter increases from $\delta = 0.5$ to $\delta = 0.8$ (1) the bifurcation point *A*, as well as the end points *B* and *C* of the unstable and stable branches, respectively, shift to lower frequencies, and (2) the ranges of frequencies (σ_B, σ_C), (σ_C, σ_A) and $(\sigma_A, 0)$ for which the system experiences pull-in from large initial deflection u_0, large steady state amplitudes on branch 3 from large initial deflection u_0, and nonzero amplitudes on branch 3, respectively, increase.

Fig. 8 illustrates the effects of the fringe parameter f on the frequency–amplitude response. Neglecting the fringe effect $f = 0$ in the model produces a significant error in the response of the microresonator given in Table 1 for which $f = 0.26$. Also, as the fringe parameter increases from $f = 0.26$ to $f = 1$, the later corresponding to a narrower beam (smaller width) and/or larger gap than Table 1, the nonlinear softening behavior increases. Moreover, the bifurcation point *A*, as well as the end points *B* and *C* of the unstable and stable branches, respectively, shift to lower frequencies. Also, the interval of frequencies for which the system reaches pull-in from higher amplitudes increases.

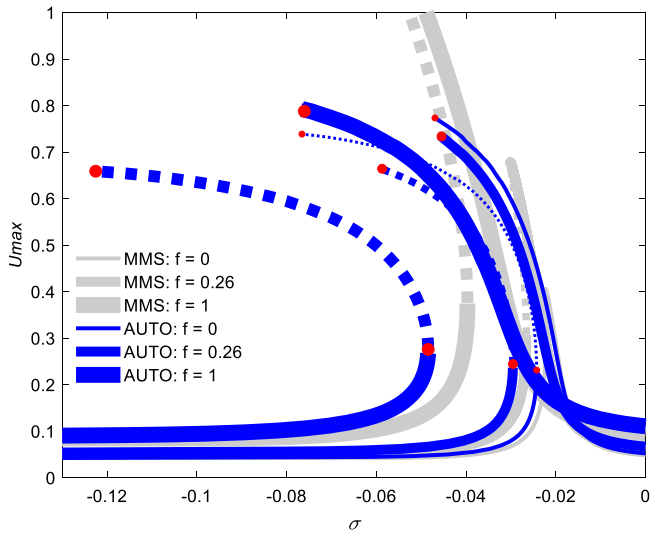

Fig. 8. Effect of voltage parameter on the frequency–amplitude response using MMS and 5T AUTO; $b^* = 0.01$, $f = 0.26$, $\omega_1 = 3.5160$, Mode 1.

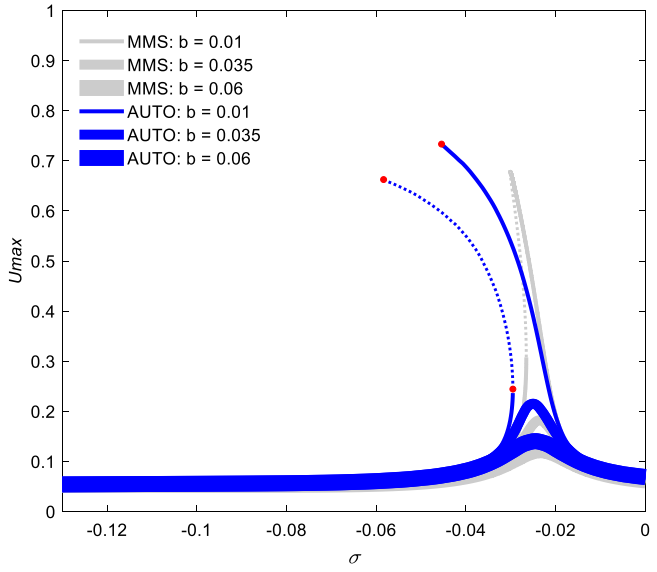

Fig. 9. Effect of fringe parameter on the frequency–amplitude response using MMS and 5T AUTO; $b^* = 0.01$, $\delta = 0.5$, $\omega_1 = 3.5160$, Mode 1.

Fig. 9 shows the effect of the damping parameter b^* on the frequency–amplitude response. At lower values of the damping parameter, the system displays a nonlinear behavior with characteristics of softening effect, while at larger values of the damping parameter displays linear dynamics characteristics. The maximum amplitude decreases with increasing the value of the damping parameter. At larger values of the damping parameter, the two branches coalesce, and the system does not experience bifurcation and pull-in phenomena.

8. Discussion and conclusions

This paper uses MMS, five-term ROM AUTO 07P (5T AUTO), five-term ROM time responses (5T TR), and BVP time responses to investigate the nonlinear frequency–amplitude response of an electrostatically actuated MEMS cantilever resonator under superharmonic resonance of the second order. There is agreement between all methods at amplitudes lower than 0.1 of the gap. At amplitudes larger than 0.1 of the gap, MMS fails to predict the behavior of the system, while all other methods make accurate predictions. The effects of the voltage δ, fringe f, and damping b^* parameters on the frequency-amplitude response are reported. The nonlinear behavior of the system is enhanced by increasing the voltage parameter and the fringe effect, and decreasing damping. Increasing the values of the voltage parameter δ and fringe parameter f results in a shift of the bifurcation branches to lower frequencies and an increase of the values of low steady-state amplitudes. The resonator does not experience any instability when damping is large enough. The predicted softening effect is in agreement with data reported in the literature [24].

In this investigation, it is assumed that the system operates under "squeeze damping in rarefied gas [29–32]. The Energy Transfer Model of the Quality Factor, Bao and Yang [29], along with the MEMS resonator characteristics in Table 1 to include the value of the Quality Factor, gives the value of damping parameter in Table 2. For the first mode of vibration, as in this paper, this corresponds to an air pressure of about 130 Pa", [19].

There are few limitations of this work. The first limitation is that this work uses Palmer's formula, to describe the fringe effect. This formula is not valid for narrow MEMS beam resonators. Therefore, these results cannot be used for narrow cantilever resonators. The structure of the MEMS resonator used for numerical simulations in this paper is wider than so called narrow structures. For narrow structures, it is recommended the use of Meijs–Fokkema, or Batra et al. [7] formulas. Batra et al. [7] formula is recommended for narrow microbeams with a width-to-thickness ratio between 0.5 and 2.0. In the present work, this ratio is 10. Ref. [7] also reported inaccurate values for Palmer's formula when the width-to-thickness and gap-to-thickness ratios are between 0.5 and 5, and 0.2 and 2, respectively. The corresponding ratios in the present work are 10 and 4, respectively. A second limitation is that no experimental work is reported. A third limitation is that the results of the present work are valid only for Euler–Bernoulli beams, i.e. slender micro-cantilevers, with a length-to-thickness ratio greater than 100, Labuschagne et al. [6]. In the present work, this ratio is 150. Therefore, the results of this work cannot be used for short cantilevers. A fourth limitation is that this work address only uniform cantilevers. For non-uniform structures, one can see Refs. [40–44] for dynamic modal characteristics of such structures and methods of finding these characteristics.

Future work could include the influence of Casimir effect in nano-electro-mechanical system (NEMS) resonators [45].

CRediT authorship contribution statement

Dumitru I. Caruntu: Conceptualization, Methodology, Software, Writing - review & editing, Supervision, Project administration, Validation, Investigation, Writing - original draft. **Martin A. Botello:** Software, Validation, Investigation, Writing - original draft. **Christian A. Reyes:** Software, Validation, Investigation, Writing - original draft. **Julio Beatriz:** Software, Validation, Investigation, Writing - original draft.

Declaration of competing interest

The authors declare that they have no known competing financial interests or personal relationships that could have appeared to influence the work reported in this paper.

References

[1] W. Zhang, M.H. Yan, Z.K. Peng, G. Meng, Electrostatic pull-in instability in MEMS/NEMS: A review, Sensors Actuators A 214 (2014) 187–218.
[2] W. Zhang, G. Meng, Nonlinear dynamical system of micro-cantilever under combined parametric and forcing excitations in MEMS, Sensors Actuators A 119 (2) (2005) 291–299.
[3] B. Milosevic, E. Farella, Wireless MEMS for wearable sensor networks, Wirel. MEMS Netw. Appl. (2017) 101–127.

[4] A. Nisar, N. Afzulpurkar, B. Mahaisavariya, A. Tuantranont, MEMS-Based micropumps in drug delivery and biomedical apllications, Sensor Actuators B 130 (2) (2008) 917–942.
[5] R.C. Batra, M. Porfiri, D. Spinello, Review of modeling electrostatically actuated microelectromechanical systems, Smart Mater. Struct 16 (2007) 23–31.
[6] A. Labuschagne, N.F.J. van Renburg, A.J. van der Merwe, Comparison of linear beam theories, Math. Comput. Modelling 49 (2009) 20–30.
[7] R.C. Batra, M. Porfiri, D. Spinello, Electromechanical model of electrically actuated narrow microbeams, J. Microelectromech. Syst. 15 (5) (2006) 1175–1189.
[8] D.I. Caruntu, M.W. Knecht, Microelectromechanical systems cantilever resonators under soft alternating current voltage of frequency near natural frequency, J. Dyn. Syst. Meas. Control 137 (4) (2015).
[9] H.L. Dai, L. Wang, Surface effect on the pull-in instability of cantilevered nano-switches based on a full nonlinear model, Physica E Low-dimens. Syst. Nanostruct. 73 (2015) 141–147.
[10] T. Mousavi, S. Bornassi, H. Haddadpour, The effect of small scale on the pull-in instability of nano-switches using DQM, Int. J. Solids Struct. 50 (9) (2013) 1193–1202.
[11] D.I. Caruntu, I. Martinez, M.W. Knecht, Reduced order model analysis of frequency response of alternating current near half natural frequency electrostatically actuated MEMS cantilevers, J. Comput. Nonlin. Dyn. 8 (2012).
[12] T. Yin, B. Wang, S. Zhou, M. Zhao, A size-dependent model for beam-like MEMS driven by electrostatic and piezoelectric forces: A variational approach, Physica E: Low-dimens. Syst. Nanostruct. 84 (2016) 46–54.
[13] M.I. Younis, E.M. Abdel-Rahman, A. Nayfeh, A reduced-order model for electrically actuated microbeam-based MEMS, J. Microelectromech. Syst. 12 (5) (2003) 672–680.
[14] S. Azizi, M.T. Chorsi, F. Bakhtiari-Nejad, On the secondary resonance of a MEMS resonator: A conceptual study based on shooting and perturbation methods, Int. J. Non-Linear Mech. 82 (2016) 59–68.
[15] D.I. Caruntu, I. Martinez, Reduced order model of parametric resonance of electrostatically actuated MEMS cantilever resonators, Int. J. Non-Linear Mech. 66 (2014) 28–32.
[16] N. Jaber, A. Ramini, Q. Hennawi, M.I. Younis, Wideband MEMS resonator using multifrequency excitation, Sensors Actuators A 242 (2016) 140–145.
[17] M.H. Ghayesh, H. Farokhi, M. Amabili, Nonlinear behaviour of electrically actuated MEMS resonators, Internat. J. Engrg. Sci. 71 (2013) 137–155.
[18] E.M. Abel-Rahman, A.H. Nayfeh, Secondary resonances of electrically actuated resonant microsensors, J. Micromech. Microeng. 13 (2003) 491–501.
[19] D.I. Caruntu, M. Botello, C.A. Reyes, J. Beatriz, Voltage-amplitude response of superharmonic resonance of second order of electrostatically actuated MEMS cantilever resonators, J. Comput. Nonlin. Dyn. 14 (3) (2019) 031005–1–031005–8, http://dx.doi.org/10.1115/1.4042017.
[20] F. Najar, A.H. Nayfeh, E.M. Abdel-Rahman, S. Choura, S. El-Borgi, Nonlinear analysis of MEMS electrostatic microactuators: Primary and secondary resonances of the first mode, J. Vib. Control 16 (9) (2010) 1321–1349.
[21] A.H. Nayfeh, M.I. Younis, Dynamics of MEMS resonators under superharmonic and subharmonic excitations, J. Micromech. Microeng. 15 (2005) 1840–1847.
[22] M.S. Al-Ghamdi, A.M. Alneamy, S. Park, B. Li, M.E. Khater, E.M. Abdel-Rahman, G.R. Heppler, M. Yavuz, Nonlinear parameter identification of a resonant electrostatic MEMS actuator, Sensors 2017 (17) (2017) 1121, http://dx.doi.org/10.3390/s17051121.
[23] F.M. Alsaleem, M.I. Younis, H.M. Ouakad, On the nonlinear resonances and dynamic pull-in of electrostatically actuated resonators, J. Micromech. Microeng. 19 (2009) 045013, 14.
[24] A. Ibrahim, N. Jaber, A. Chandran, M. Thirupathi, M. Younis, Dynamics of microbeams under multi-frequency excitations, Micromachines 8 (32) (2017) 14, http://dx.doi.org/10.3390/mi8020032.
[25] A.H. Nayfeh, M.I. Younis, E.M. Abel-Rahman, Reduced-order models for MEMS applications, Nonlinear Dynam. 41 (2005) 211–236.
[26] D.I. Caruntu, M. Knecht, On nonlinear response near-half natural frequency of electrostatically actuated microresonators, Int. J. Struct. Stab. Dyn. 11 (4) (2011) 641–672.
[27] D.I. Caruntu, I. Martinez, K.N. Taylor, Voltage-amplitude response of alternating current near half natural frequency electrostatically actuated MEMS resonators, Mech. Res. Commun. 52 (2013) 25–31.
[28] M.I. Younis, MEMS Linear and Nonlinear Statics and Dynamics, Springer, New York, 2011.
[29] M. Bao, H. Yang, Squeeze film air damping in MEMS, Sensors Actuators A 136 (2007) 3–27.
[30] C.C. Nguyen, W.L. Li, Effect of gas on the quality factors of micro-beam resonators, Microsys. Technol. 23 (2017) 3185–3199.
[31] X. Guo, A. Alexeenko, Compact model on rarefied flow simulations, J. Micromech. Microeng. 19 (2009) 045026, 7.
[32] J.W. Lee, R. Tung, A. Raman, H. Sumali, J.P. Sullivan, Squeeze-film damping of flexible microcantilevers at low ambient pressures: theory and experiments, J. Micromech. Microeng. 19 (2009) 105029, 14.
[33] A.H. Nayfeh, D.T. Mook, Nonlinear Oscillations, Wiley, New York, 1979.
[34] S.K. Dwivedy, R.C. Kar, Nonlinear response of a parametrically excited system using higher-order method of multiple scales, Nonlinear Dynam. 20 (1999) 115–130.
[35] D.I. Caruntu, I. Martinez, M.W. Knecht, Parametric resonance voltage response of electrostatically actuated micro-electro-mechanical system cantilever resonators, J. Sound Vib. 362 (2016) 203–213.
[36] E.J. Doedel, B.E. Oldeman, AUTO-07P: Continuation and Bifurcation Software for Ordinary Differential Equations, Concordia University, Montreal, Canada, 2012.
[37] L.F. Shampine, M.W. Reichelt, The MATLAB ODE suite, SIAM: J. Sci. Comput. 18 (1997) 1–22.
[38] L.F. Shampine, M.W. Reichelt, J.A. Kierzenka, Solving index-1 DAEs in MATLAB and simulink, SIAM Rev. 41 (1999) 538–552.
[39] J.A. Kierzenka, L.F. Shampine, A BVP solver based on residual control and the MATLAB PSE, ACM Trans. Math. Software 27 (3) (2001) 299–316.
[40] D.I. Caruntu, Classical Jacobi polynomials, closed-form solutions for transverse vibrations, J. Sound Vib. 306 (3–5) (2007) 467–494.
[41] D.I. Caruntu, Dynamic modal characteristics of transverse vibrations of cantilevers of parabolic thickness, Mech. Res. Commun. 33 (3) (2009) 391–404.
[42] D.I. Caruntu, Self-adjoint differential equations for classical orthogonal polynomials, J. Comput. Appl. Math. 180 (1) (2005) 107–118.
[43] D.I. Caruntu, Factorization of self-adjoint ordinary differential equations, Appl. Math. Comput. 219 (1) (2013) 7622–7631.
[44] D.I. Caruntu, Eigenvalue singular problem of factorized fourth-order self-adjoint differential equations, Appl. Math. Comput. 224 (1) (2013) 603–610.
[45] D.I. Caruntu, C.A. Reyes, Casimir effect on amplitude–frequency response of parametric resonance of electrostatically actuated NEMS cantilever resonators, in: B.E. Abali, I. Giorgio (Eds.), Chapter 15 in Developments and Novel Approaches in Nonlinear Solid Body Mechanics – Book Series Advanced Structured Materials, Vol.132, Springer Nature Switzerland AG, Gewerbestrasse 11, 6330 Cham, Switzerland, 2020, pp. 237–259, http://dx.doi.org/10.1007/978-3-030-50464-9_15.